Environmental Pollution 237 (2018) 228–236

Contents lists available at ScienceDirect

Environmental Pollution

journal homepage: www.elsevier.com/locate/envpol

Enhanced immobilization of U(VI) on *Mucor circinelloides* in presence of As(V): Batch and XAFS investigation☆

Wencheng Song [a, b], Xiangxue Wang [b], Zhongshan Chen [b], Guodong Sheng [b, c], Tasawar Hayat [d], Xiangke Wang [b, d, e], Yubing Sun [b, *]

[a] Anhui Province Key Laboratory of Medical Physics Technology and Center of Medical Physics and Technology, Hefei Institutes of Physical Sciences and Hefei Cancer Hospital, Chinese Academy of Sciences, Hefei 230031, PR China
[b] College of Environmental Science and Engineering, North China Electric Power University, Beijing 102206, PR China
[c] College of Chemistry and Chemical Engineering, Shaoxing University, Zhejiang 312000, PR China
[d] Collaborative Innovation Center of Radiation Medicine of Jiangsu Higher Education Institutions and School for Radiological and Interdisciplinary Sciences, Soochow University, 215123, Suzhou, PR China
[e] NAAM Research Group, Faculty of Science, King Abdulaziz University, Jeddah 21589, Saudi Arabia

ARTICLE INFO

Article history:
Received 27 September 2017
Received in revised form
16 January 2018
Accepted 19 February 2018

Keywords:
Reduction
Trögerite
Antioxidase
Thiol compounds
Organic acid

ABSTRACT

The combined pollution of radionuclides and heavy metals has been given rise to widespread concern during uranium mining. The influence of As(V) on U(VI) immobilization by *Mucor circinelloides* (*M. circinelloides*) was investigated using batch experiments. The activity of antioxidative enzymes and concentrations of thiol compounds and organic acid in *M. circinelloides* increased to respond to different U(VI) and As(V) stress. The morphological structure of *M. circinelloides* changed obviously under U(VI) and As(V) stress by SEM and TEM analysis. The results of XANES and EXAFS analysis showed that U(VI) was mainly reduced to nano-uraninite (nano-UO_2, 30.1%) in U_{400}, while only 9.7% of nano-UO_2 was observed in the presence of As(V) in U_{400}-As_{400} due to the formation of uranyl arsenate precipitate (Trögerite, 48.6%). These observations will provide the fundamental data for fungal remediation of uranium and heavy metals in uranium-contaminated soils.

© 2018 Elsevier Ltd. All rights reserved.

1. Introduction

With the rapid development and application of nuclear energy, demands for uranium (U) resources will greatly increase in the next few decades. A large number of radionuclides and heavy metals are produced during uranium mining and tailings disposal, which cause the combined pollution of radionuclides and heavy metals in the surrounding environment (Dresel et al., 2011; Sitte et al., 2010). The U content in the contaminated water is 1–3 orders of magnitude higher than that in ordinary water (Richard et al., 2012). The content of arsenic (As) in U ore is 1.2–10% (~6 g/kg), which is one of the main heavy metal pollution elements in U tailings (Chen et al., 2006; Troyer et al., 2014a). U and As are multi-valence elements, and chemical properties of them are very active. U(VI) and As(V) as mainly oxidized states are highly toxic, easily soluble in natural waters and soils (non-reducing environments), presenting high risks to the environment because of radioactive poisoning or chemical poisoning. In additions, the migration and diffusion of soluble U(VI) and As(V) result in serious environmental pollution around the mining area and downstream areas (Liber et al., 2011; Rodríguez-Lado et al., 2013; Schnug and Lottermoser, 2013). Therefore, it is necessary to study the mutual effect of U(VI) and As(V) in the pollution.

Owing to the prevalence in nature, fungi have been used as high efficient adsorbents for the removal of radionuclides and heavy metals in environmental remediation (Das, 2012; Gadd, 2010; Harms et al., 2011). For example, approximately 99.9% and 97.1% of U(VI) was removed by *Trichoderma harzianum* and algae, respectively (Akhtar et al., 2007). Ding et al. (2014a,b) found that *Geotrichum sp.* dwc-1 (5 g/L) had a good scavenging effect on thorium (*Kd* as high as 0.93 mL/mg). Hansen et al. (2006) found that the maximum adsorption capacities of As(V) on *Lessonia nigrescens* was 45.2 mg/g at pH = 2.5. However, to the authors' knowledge, few studies regarding the simultaneous adsorption of U(VI) and As(V) on fungi are available nowadays.

☆ This paper has been recommended for acceptance by Dr. Jorg Rinklebe.
* Corresponding author.
E-mail address: sunyb@ipp.ac.cn (Y. Sun).

https://doi.org/10.1016/j.envpol.2018.02.060
0269-7491/© 2018 Elsevier Ltd. All rights reserved.

Radionuclides and heavy metals have strong oxidative properties. Therefore, radionuclides and heavy metals ions can produce large amounts of reactive oxygen species when they enter the cell (Baldrian, 2003; Gutiérrez, 2009; Zhu et al., 2016), which destroys different kinds of biomolecules, and even can lead to cell death. To avoid the negative effects of reactive oxygen species, fungi have evolved an antioxidative defense mechanism consisting of non-enzymatic/enzymatic components such as oxalic, citric acid (Arwidsson et al., 2010; Boriová et al., 2016; Martin et al., 2012), superoxide dismutases (SOD) and catalase (CAT) (Xu et al., 2011; Schneider et al., 2017), as well as thiol compounds (e.g., non-protein thiols (NP-SH) and protein thiols (PB-SH)) (Xu et al., 2014, 2017). Among these chelating compounds, oxalic acid and citric acid as two major secretions produced by fungi can fix, stabilize and detoxify heavy metals (Mäkelä et al., 2010; Vázquez-Campos et al., 2015; Wei et al., 2012; Xu et al., 2015). In addition, oxalic and citric acids produced from fungi as the leaching agent can increase efficiency of U extraction (Desouky et al., 2016; Wang et al., 2013). Apart from chelation and co-precipitation, the fungal reduction of U(VI) to uraninite (UO_2) is usually considered to be a tactic for U(VI) bioremediation (Wall and Krumholz, 2006; Wu et al., 2006, 2007). However, these studies focused on fungal single sorption radionuclides or heavy metals.

Mucor circinelloides Tiegh., 1875 (*M. circinelloides,* as a typical fungus) was used in this study due to its ubiquity in radionuclides' contaminated soils. The objectives of this study were to (1) investigate the change of antioxidative capacity (SOD, CAT), thiol compounds (NP-SH and PB-SH), and organic acid (oxalic, citric acid) of *M. circinelloides* under different U(VI) and As(V) stress by the batch technique; (2) determine the interaction mechanism of U(VI) and As(V) in *M. circinelloides* by X-ray absorption spectrometry (XAFS), including X-ray absorption near edge structure (XANES) and extended X-ray absorption fine structure (EXAFS) spectra.

2. Materials and methods

2.1. Materials

The U(VI) and As(V) stock solution (0.1 M) was prepared from uranium nitrate ($UO_2(NO_3)_2 \cdot 6H_2O$, 99.99% purity, Sigma-Aldrich) and sodium arsenate ($Na_2HAsO_4 \cdot 7H_2O$, 99.99% purity, Sigma-Aldrich) after dissolution and dilution with Milli-Q water, respectively. The standard of biogenic UO_2 used in this study was synthesized according to Ulrich et al. (2008). The XAFS data of $UO_2HAsO_4 \cdot 4H_2O$ standard was derived from Troyer et al. (2014a,b). Oxalic and citric acid (HPLC grade) standard was purchased from Sigma-Aldrich Co. All other reagents (Sinopharm Chemical Reagent Co., Ltd., Shanghai, China) were used directly without further purification in this study.

2.2. Cultivation of resistant fungus

Resistant fungus used in this study was earlier isolated from radionuclide-contaminated soils, and resistant fungus was cultured in Czapek-Dox medium (20 g sucrose, 2 g $NaNO_3$, 0.7 g KH_2PO_4, 0.3 g K_2HPO_4, 0.5 g KCl, 0.5 g $MgSO_4 \cdot 7H_2O$, all dissolved in 1000 mL distilled water) and identified as *M. circinelloides* using the molecular biology methods (Song et al., 2016a). The metal tolerance of fungal communities was increased after exposure to metals, resulting from the decrease of metal sensitive fungal population and subsequent competition and high adaptation potential of surviving fungi (Gadd, 2010; Zhang et al., 2005). Cultivation of the fungus was carried out in 250 mL Erlenmeyer flasks with 100 mL growth medium on a rotary shaker (SHZ-82A, Ronghua Instrument Technology Co., Jin Tan City, China) at 200 rpm and 28 °C. After 3 days' cultivation, mycelia were harvested by centrifugation, washed three times in deionized water and stored at 4 °C for batch experiments. Besides, the dry weight of fungal biomass was determined after drying at 70 °C for 3 days.

2.3. Characterization

The morphologies of U(VI) and/or As(V) loaded *M. circinelloides* were characterized by JSM-6320F Scanning Electron Microscope (SEM, JEOL, Tokyo, Japan) and HT-7700 Transmission Electron Microscope with an energy dispersive X-ray analysis (EDX) (TEM, Hitachi High-Technologies Co. Ltd., Tokyo, Japan). *M. circinelloides* was inoculated on Czapek-Dox liquid medium in 250 mL Erlenmeyer flasks at pH 5.5 containing 200 μM U(VI), 400 μM U(VI), 400 μM U(VI) and 200 μM As(V) (noted as U_{200}, U_{400} and U_{400}-As_{200}, respectively), the absence of U(VI) and As(V) was treated as control, and fungal mycelia were collected after 3 days. Then, the U(VI) and/or As(V)-loaded *M. circinelloides* were fixed in 5% glutaraldehyde at 4 °C for 4 h, washed with 0.1 M phosphate buffer and then dehydrated sequentially in 10, 30, 70, 90 and 100% ethanol, finally critical-point-dried, gold-coated with stubs for SEM analysis. Whereas, the samples for TEM were prepared by fixing sample into 5% glutaraldehyde for 3 h, then post-fixing in 1.0% osmium tetraoxide for 2 h and then by dehydrating it in a graded ethanol series (50%–100%). Finally, mycelia were sectioned, and stained for TEM analysis. U L_{III}-edge XANES and EXAFS spectra were collected at Shanghai Synchrotron Radiation Facility (BL14W, Shanghai, China). Electron storage ring energy and the maximum storage beam current were 3.5 GeV and 210 mA, respectively. A multi-element pixel high purity Ge solid-state detector was used to collect the fluorescence signal. The samples for XANES and EXAFS spectra were followed: the Czapek-Dox liquid medium containing different U(VI) and As(V) concentrations and mycelia were added into 250 mL flask bottles at 28 °C for 3 days, and then fungal mycelia and precipitations were collected by centrifuging and washing with sterile deionized water. The detailed experimental conditions were summarized in Table 1. The standard UO_2 and $UO_2HAsO_4 \cdot 4H_2O$ were used as references for XAFS evaluation. The linear combination fitting (LCF) was analyzed using SixPACK software (Stylo et al., 2013; Troyer et al., 2014a), and the data of EXAFS were analyzed using IFFEFIT 7.0 software (Sheng et al., 2016; Sun et al., 2014). The coordination number (CN), interatomic distance (R), and Debye–Waller factor (σ^2) were allowed to float as adjustable parameters.

2.4. Batch immobilization experiments

The batch immobilization of U(VI) and As(V) by mycelia were carried out under ambient conditions in triplicate. Briefly, 0.6 g fungal cells were slowly added to the 100 mL different

Table 1
Experimental conditions of fungi mycelia with different U(VI) and As(V) concentrations.

Samples	U(VI) (μM)	As(V) (μM)	Culture time (h)	XAFS collected
U_{40}	40		72	
U_{400}	400		72	✓
As_{40}		40	72	
As_{400}		400	72	
U_{40}-As_{40}	40	40	72	
U_{40}-As_{200}	40	200	72	
U_{40}-As_{400}	40	400	72	
U_{400}-As_{40}	400	40	72	✓
U_{400}-As_{200}	400	200	72	✓
U_{400}-As_{400}	400	400	72	✓

concentrations of U(VI) and As(V) in 250 mL Erlenmeyer flasks to determine the accumulation capacity of mycelia. The controlled experiments were also conducted the same experimental condition without U(VI) or As(V) solution. The suspensions were pH adjusted to 5.5, and then were reacted for 72 h under stirring conditions. After removal equilibrium, mycelia were collected by centrifugation at 6000 rpm for 15 min. The content of U(VI) and/or As(V) was analyzed with an inductively coupled plasma-atomic emission spectroscopy (ICP-AES 300, Thermo Fisher Scientific, USA). The detection limits were 0.5×10^{-6} M for U and 0.2×10^{-6} M for As. The immobilization percentage and amounts of U(VI) and As(V) were described as Eqns. (1) and (2), respectively:

$$\text{Immobilization } \% = (C_0\text{-}C_e) \times 100\% / C_0 \quad (1)$$

$$Q = (C_0\text{-}C_e) \times V/m \quad (2)$$

Where C_0 and C_e (mg/L) were initial and equilibrium concentrations, respectively. m and V were the mass of mycelia and volume of suspension, respectively.

2.5. Estimation of fungal components

The estimation of fungal components under different culture time (0–144 h) after U(VI) and As(V) exposure were performed at T = 301 K and pH = 5.5. Briefly, 2.0 g fresh mycelia were frozen using liquid nitrogen and ground into powder, and then 10 mL of extraction solution (50 mM sodium phosphate, 1% PVP, and 0.1 mM EDTA) was added. After that, SOD activity was monitored by measuring its ability to inhibit photochemical reduction of nitro blue tetrazolium at 560 nm (Rico et al., 2013), and CAT activity was assayed by measurement of the decrease of absorbance at 240 nm (Zhang et al., 2016).

The NP-SH concentration was analyzed by UV2550 UV–Vis spectrophotometer (Shimadzu, Kyoto, Japan) at 412 nm, whereas the concentration of PB-SH was obtained by the difference of total thiols and NP-SH. For total thiols, 0.1 mL of above extracts were mixed with 0.3 mL of 0.2 M Tris, and 0.02 mL of 0.01 M DTNB, and then the mixtures were brought to 2.0 mL with absolute methanol for 15 min. For NP-SH, 1 mL of fungal extracts were mixed with 0.8 mL deionized water and 0.2 mL of 50% trichloroacetic acid. Afterwards, the solution was mixed with 4 mL of 0.4 M Tris and 0.1 mL of 0.01 M DTNB, and then was centrifuged it at 6000 rpm for 10 min (Guimarães-Soares et al., 2007).

The concentrations of oxalic and citric acid were determined by Agilent 1260 high-performance liquid chromatography (HPLC) (Agilent Technologies Inc., California, USA) consisting of a G1314B 1260 VWD VL detector at 210 nm (Li et al., 2011). The mobile phase was phosphoric acid (0.2% v/v). 2 mL of fungal supernatant was collected at different time, and then was centrifuged at 6000 rpm for 10 min. Oxalic and citric acid was identified by comparing the retention time of each standard (Montiel-Rozas et al., 2016). Under these conditions (e.g., a signal-to-noise ratio of 3), the detection limits of this method were 2.0×10^{-7} M for oxalic acid and 1.0×10^{-7} M for citric acid. All tests were conducted in triplicate.

2.6. Statistical analysis

Statistical analysis was performed with the computer programs of SPSS in version 19.0 (Statistical Package for Social Science, Inc., IL, USA). The data obtained from at least three independent experiments were presented as means ± S.D. The fulfilment of the one-way analysis of variance (ANOVA) requirements, specifically the normal distribution of the residuals and the homogeneity of variance, was tested by means of the Shapiro–Wilk's and the Levene's tests, respectively. Statistical significances between groups were evaluated by ANOVA with a Student-Newman-Keuls post-test (if data fulfilled homoscedasticity) or Tamhane's T2 post-test (if data did not fulfill homoscedasticity). A p-value < 0.05 between two independent groups was considered to the statistically significant difference. In addition, the error bars (<5%) were provided in this study.

3. Results and discussion

3.1. Morphological analysis

The morphologies of *M. circinelloides* before and after U(VI)/As(V) immobilization were illustrated by SEM and TEM patterns. Compared with raw fungal mycelia (Fig. 1a), the samples of U_{200} and U_{400}-As_{200} displayed obviously more plump and less sporangium (Fig. 1b and c), while the cell wall of U_{400} seemed to be broken and lesser sporangium, the most serious damage of *M. circinelloides* (indication with red arrow) (Fig. 1d) (El-Sayed, 2015; Song et al., 2016b). The less damage of *M. circinelloides* after addition of 400 μM U(VI) and 200 μM As(V) solution could be attributed to the co-precipitation of As(V) and U(VI). General, the co-precipitates were deposited of extracellular *M. circinelloides,* resulting in the decrease of bioavailability. In order to further investigate the changes of subcellular structure, the morphologies of *M. circinelloides* under 400 μM U(VI) stress were conducted by TEM patterns, and the absence of U(VI) was treated as control. As shown in Fig. 1e and f, *M. circinelloides* after addition of U(VI) showed a distorted cellular structure and a slightly compacted cell. The black precipitates with a high electron density (indication with red arrow in Fig. 1f) around the cell walls of *M. circinelloides* after U(VI) exposure. The EDX spectra derived from electron-dense bodies indicated that they were consisted of carbon, oxygen, phosphorus, uranium and copper. The copper band was from the grid used to support sections. Srivastava and Thakur (2006) demonstrated that the intracellular electron-dense area of *Aspergillus niger* was attributed to the penetration of chromate into the cell by TEM observations. Liu and Kottke (2004) also found that excess Cu(II) induced ultrastructural changes of *Allium sativum* L. such as strong vacuolization, condensed nuclear chromatin, decreased endoplasmic reticulum and ribosome and serious plasmolysis.

3.2. Analysis of biomass weight

Fig. 2a shows the effect of U(VI)/As(V) concentration on biomass weights of fungal mycelia under different culture time. The biomass weight of fungal mycelia increased rapidly within 60 h, whereas the biomass weight of U_{200}, U_{400} and U_{400}-As_{200} samples slightly decreased after culture time more than 80 h. The biomass weights of fungal mycelia in decreasing order were: U_0, U_{200}, U_{400}-As_{200} and U_{400} with significant differences of U_{400}-As_{200}, and U_{400} versus U_0 ($p < 0.05$). The biomass weight of U_{400}-As_{200} was more lower than that of U_{400}, suggesting that the complex of U(VI) with As(V) resulted in the decrease of damage for *M. circinelloides* (Brooks et al., 2003).

3.3. Analysis of antioxidase activity

The SOD and CAT activity of *M. circinelloides* under different culture time was shown in Fig. 3a and b, respectively. As shown in Fig. 3a, the SOD activity increased gradually with increasing culture time within 72 h, and then slight increase was observed after 72 h. However, the CAT activity increased progressively with increasing culture time. The activity of SOD and CAT in U_{400} were greater than that of U_0, U_{200} and U_{400}-As_{200}, and significant differences were

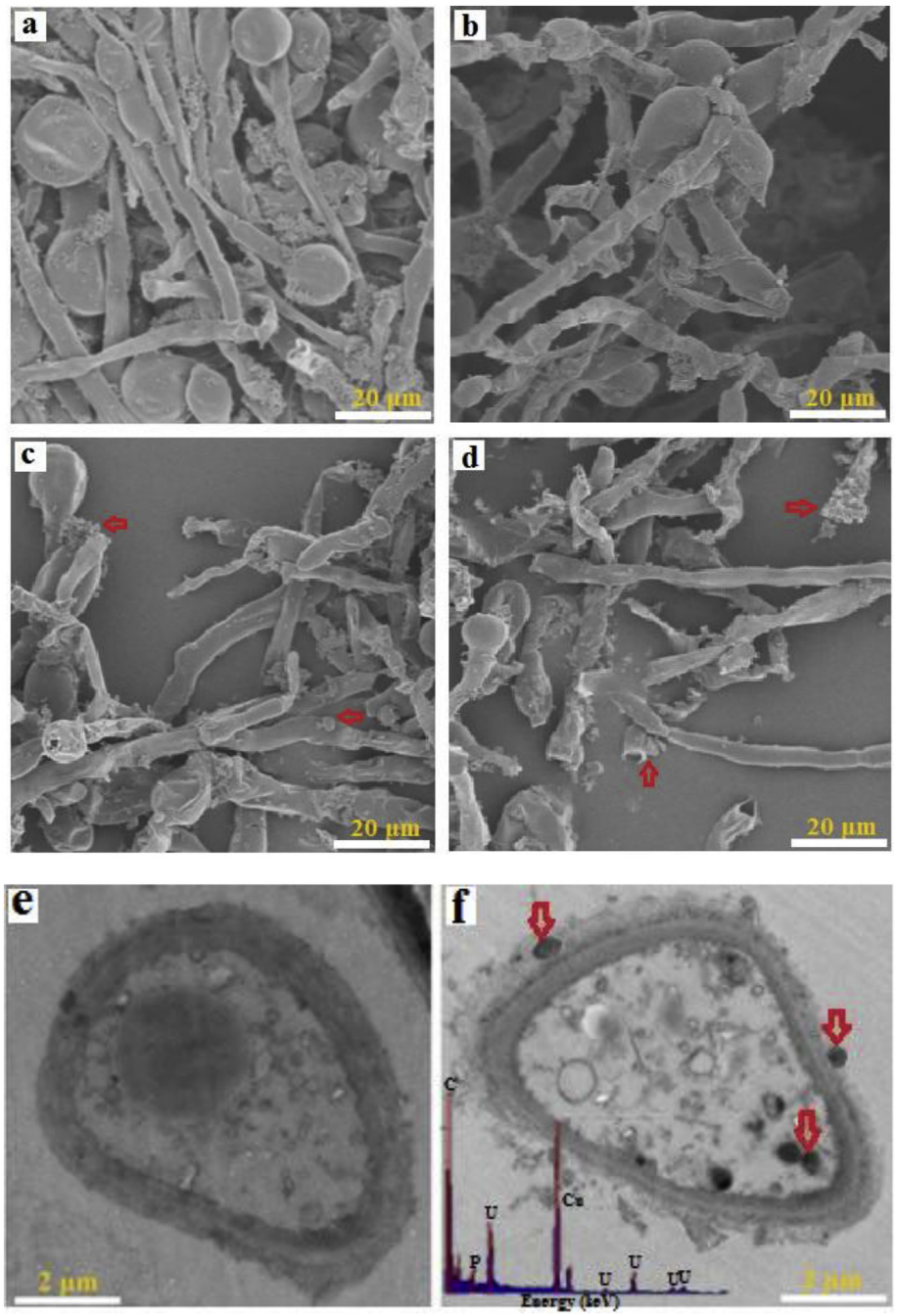

Fig. 1. Characterization of *M. circinelloides* with U(VI)/As(V) immobilization, (a)–(d): SEM images of U_0, U_{200}, U_{400}-As_{200} and U_{400}, (e) and (f): TEM images of U_0 and U_{400}, respectively.

observed in U_{200}, U_{400}-As_{200}, and U_{400} versus U_0 ($p < 0.05$), which was consistent with results of biomass weight. Xu et al. (2011) found that SOD and CAT activities in *Agaricus bisporus* were significantly increased after long-term exposure to heavy metals such as Cd(II), Pb(II) and Cu(II). Yin et al. (2016) also demonstrated that SOD could partially limit the formation of Ag nanoparticles by *F. oxysporum*, demonstrating the critical role of superoxide in the reduction of silver. Besides, Cu-induced oxidative stress increased the activity of SOD and CAT in *arbuscular mycorrhizal*, resulting in the decrease of oxidative damage to lipids (Azevedo et al., 2007).

3.4. Analysis of thiol compounds

Fig. 4a and b shows the effect of U(VI)/As(V) concentration on levels of NP-SH and PB-SH under different culture time, respectively. The concentrations of NP-SH and PB-SH for U_{200}, U_{400}-As_{200} and U_{400} were distinctly higher than that of U_0 with significant differences ($p < 0.05$). Within exposure of 72 h, the concentrations of NP-SH and PB-SH increased rapidly with increasing culture time, whereas NP-SH and PB-SH contents decreased slowly after 72 h exposure. The main mechanisms of metal detoxification appear to involve the chelation of metal ions in the cytosol with thiol-containing compounds. Thiol-containing compounds are divided

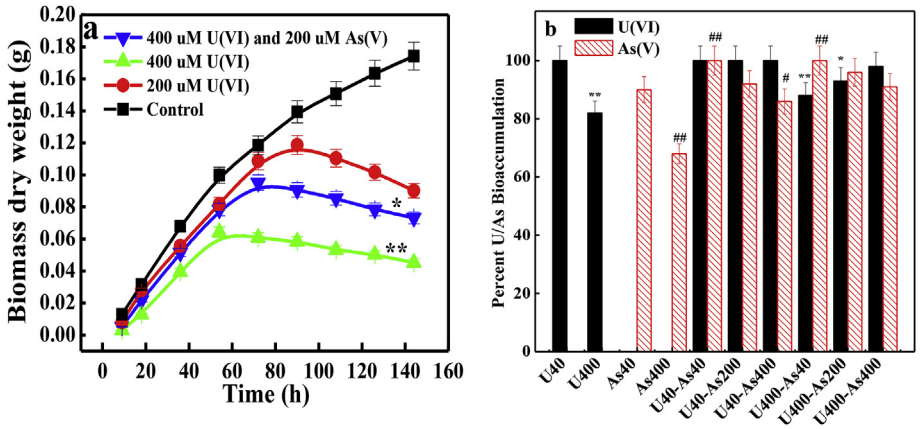

Fig. 2. a: effect of U(VI) and/or As(V) concentration on biomass weights of fungal mycelia under different culture time, T = 301 K and pH = 5.5. The normality and homoscedasticity of the data were verified using the Shapiro-Wilk and Levene's tests, and the homoscedastic data were analyzed by ANOVA with Student Newman-Keuls, *: $p < 0.05$, **: $p < 0.01$ versus the control. b: Bioaccumulation of U(VI) and As(V) on fungi mycelia under different U(VI)/As(V) concentrations, T = 301 K and pH = 5.5. Data represent the means ± SD of three independent experiments. *: $p < 0.05$, **: $p < 0.01$ versus U40, #: $p < 0.05$, ##: $p < 0.01$ versus As40, by ANOVA, Student Newman-Keuls.

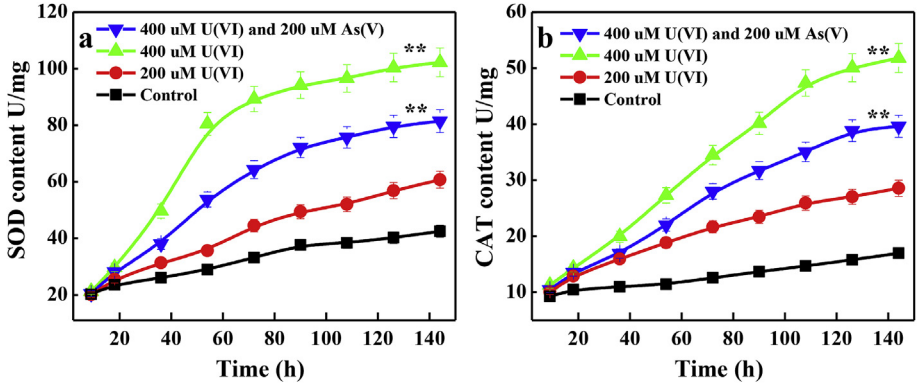

Fig. 3. Effect of U(VI)/As(V) concentration on the concentrations of SOD (a) and CAT (b) under different culture time. T = 301 K and pH = 5.5. The normality and homoscedasticity of the data were verified using the Shapiro-Wilk and Levene's tests, and the heteroscedastic data with Tamhane's T2, *: $p < 0.05$, **: $p < 0.01$ versus the control.

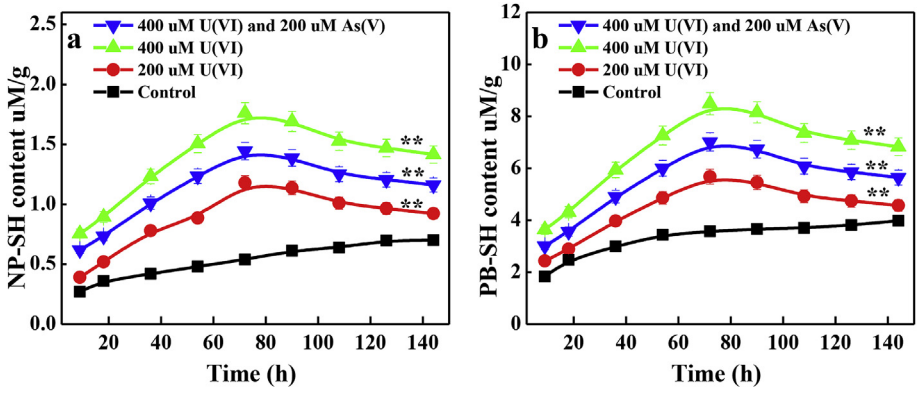

Fig. 4. Effect of U(VI)/As(V) concentration on the concentrations of NP-SH (a) and PB-SH (b) under different culture time, T = 301 K and pH = 5.5. The normality and homoscedasticity of the data were verified using the Shapiro-Wilk and Levene's tests, and the homoscedastic data were analyzed by ANOVA with Student Newman-Keuls, *: $p < 0.05$, **: $p < 0.01$ versus the control.

into non-protein thiols (NP-SH) and protein thiols (PB-SH) according to the molecular weight and combination. PB-SH is thiol on the protein, whereas NP-SH is free thiol compounds in cell such as glutathione, phytochelatins, or metallothioneins. The increase of intracellular thiol compounds was a protection mechanism of *M. circinelloides* to deal with the hazards of U(VI)/As(V) (Song et al., 2016b). The detoxification of U(VI) by *M. circinelloides* may be partially mediated by thiol coordination to decrease metabolic processes damage (Zhan et al., 2015). Certainly, indications of harmful effects of U(VI)/As(V) exposure was related to the microscopy (seemingly damaged fungi), SOD and CAT activity (possibly indicating stress) and the highest reduction in biomass. Li et al.

(2015) also demonstrated that the thiol compounds of *P. chrysosporium* presented an extracellular defense for Pb(II) due to the coordination of Pb(II) with -SH groups of thiol compounds, resulting in the decrease of damage during metabolic processes (Li et al., 2015). Therefore, the concentrations of NP-SH and PB-SH significantly increased with increasing U(VI) concentration to enhance extracellular defense for U(VI) (Zhan et al., 2015). However, the decreased concentrations of NP-SH and PB-SH after addition of As(V) could be ascribed to the formation of uranyl-arsenic co-precipitates, resulting in the decrease of the free available U(VI) concentration. NP-SH and PB-SH could take part in reduction of U(VI) to U(IV) due to its strong reducibility (Song et al., 2016b). Generally, the higher constitutive levels of heavy metals leads to the higher production capacity of thiol compounds, resulting in the more rapid response when exposed to heavy metals (Guimarães-Soares et al., 2007).

3.5. Analysis of organic acids

Fig. 5a and b showed the effect of U(VI)/As(V) concentration on the oxalic and citric acid, respectively. The concentrations of oxalic and citric acids slightly increased within 24 h exposure, and then a significant increase of oxalic and citric acids was observed after 24 h exposure. The concentrations of citric and oxalic acids in U_{400} were significantly higher than that of U_0, U_{200} and U_{400}-As_{200} with significant differences of U_{400}-As_{200}, and U_{400} versus U_0 ($p < 0.05$), suggesting that organic acids played a great role in bioaccumulation of U(VI) and As(V). These organic acids could be used as electron donor and/or acceptor to facilitate the reduction of U(VI) to U(IV) (e.g., nano-UO_2(s)) in the absence of As(V). The addition of As(V) decreased generation of organic acid, suggesting the formation of uranyl arsenate precipitates. Wall and Krumholz (2006) determined Cd(II)-oxalate complex in *Phanerochaete chrysosporium*. Grąz et al. also demonstrated an increase of oxalic acid in *Abortiporus biennis* and *Bjerkandera fumosa* under heavy metals stress (Grąz et al., 2009; Grąz and Jarosz-Wilkołazka, 2011). Therefore, these organic acids produced from fungi significantly influenced the mobilization of U(VI) and As(V) due to the formation of metal complexes (Arwidsson et al., 2010). Ding et al. (2014a,b) also showed that the extraction of Pb, Cd, Zn and Cu from the acid mine soil in the presence of organic acids (acetic, oxalic, malic, fumaric, tartaric and citric acids) at pH 7 was much higher than that extraction amount from the alkaline mine soil. Compared to oxalic acid, citric acid at high concentration was capable of extracting these heavy metals due to the strong ability with heavy metals. Xu et al. demonstrated that the addition of oxalic acid alleviated the toxicity of Cd and increased its bioavailability (Xu et al., 2015).

3.6. Enhanced U(VI) immobilization by As(V)

Fig. 2b shows the bioaccumulation of U(VI)/As(V) on *M. circinelloides* under the different U(VI)/As(V) conditions. For the single-solute system, the bioaccumulation of U(VI)/As(V) significantly decreased with increasing U(VI)/As(V) concentration. For example, approximate 100% of U(VI) and 90% of As(V) were accumulated on the surface of fungi mycelia at low concentrations (40 μM), whereas ~ 80% of U(VI) and 70% of As(V) were accumulated at high initial concentrations (400 μM). For the U-As system, bioaccumulation of As(V) decreased from 99% (U_{40}-As_{40}) to 86% (U_{40}-As_{400}) as the increase of As(V) dosage, whereas approximate 100% of U(VI) was still accumulated on the surface of fungi mycelia at low U(VI) concentrations (40 μM). At high initial U(VI) concentration (400 μM), the bioaccumulation of U(VI) increased with increasing As(V) concentration, whereas the decrease of As(V) bioaccumulation was observed. It was noted that the decreased extent of As(V) at U-As system (90% and 95% for U_{40}-As_{400} and U_{400}-As_{400}, respectively) was significantly lower than that of single As system (70% for As_{400}), which indicated that U(VI) also enhanced As(V) bioaccumulation on surface of fungi mycelia. In addition, the bioaccumulation of U(VI) in the presence of As(V) was not influenced by their speciation. As shown in Fig. S1 of SI, the main U(VI) and As(V) speciation at pH < 5.5 was UO_2^{2+} and $H_2AsO_4^{2-}$ species, respectively. The pH values during the growth medium of the mycelia were less than 5.5 (Fig. S2). Therefore, the main species of U(VI) and As(V) during the growth medium of the mycelia were UO_2^{2+} and $H_2AsO_4^{2-}$ species, respectively.

3.7. XANES and EXAFS analysis

U L_{III}-edge XANES spectra of standard (UO_2 and $UO_2HAsO_4 \cdot 4H_2O$) and U-containing samples (U_{400}, U_{400}-As_{40}, U_{400}-As_{200} and U_{400}-As_{400}) were presented in Fig. 6a. The absorption edge energies at 17175 eV and 17178 eV corresponded to nano-UO_2 and $UO_2HAsO_4 \cdot 4H_2O$ standards, respectively (Blake et al., 2015; Ding et al., 2015; O'Loughlin et al., 2010; Sun et al., 2016; Troyer et al., 2014b). It was observed that adsorption-edge energies of U_{400} were very close to nano-UO_2 reference, indicating that the accumulated U(VI) was reduced to U(IV) by thiol compounds produced from the fungi at high U(VI) concentrations. However, the adsorption edges of U_{400}-As_{40}, U_{400}-As_{200} and U_{400}-As_{400} were shifted to the high energy with increasing As(V) concentrations, revealing that speciation of uranium in fungal mycelia was transformed with the increase of As(V) dosage. The adsorption energy of U_{400}-As_{400} was consistent with $UO_2HAsO_4 \cdot 4H_2O$ standards, indicating the formation of uranyl-arsenate precipitate

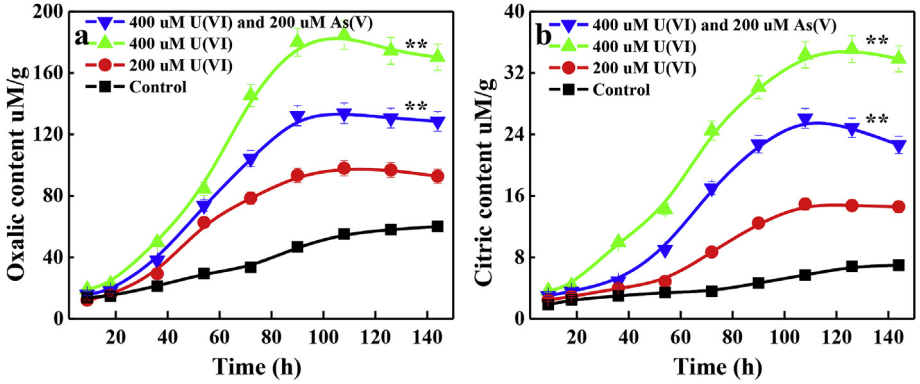

Fig. 5. Effect of U(VI)/As(V) concentration on the concentrations of oxalic acid (a) and citric acid (b) under different culture time, T = 301 K and pH = 5.5. The normality and homoscedasticity of the data were verified using the Shapiro-Wilk and Levene's tests, and the heteroscedastic data with Tamhane's T2, *: $p < 0.05$, **: $p < 0.01$ versus the control.

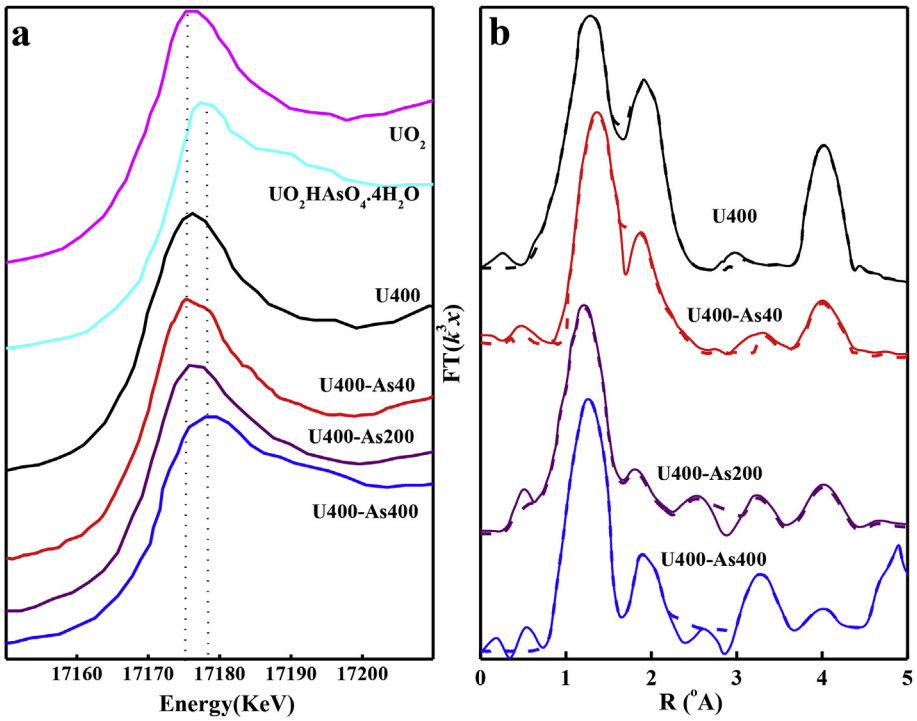

Fig. 6. Uranium L_{III}-edge XANES (a) and EXAFS (b) spectra of U(VI) bioaccumulation in *M. circinelloides* at different groups, Solid and dash lines represent experimental spectra and spectral fits, respectively.

($UO_2HAsO_4 \cdot 4H_2O$) under the high U(VI) and As(V) concentration. Table 2 summarized the contents of nano-UO_2, U(VI) accumulated to biomass, and $UO_2HAsO_4 \cdot 4H_2O$ in U_{400}, U_{400}-As_{40}, U_{400}-As_{200} and U_{400}-As_{400} samples calculated from LCF method. For U_{400}, approximate 30% nano-UO_2 and 70% U(VI) were accumulated on surface of fungi mycelia, whereas only 9.7% of nano-UO_2 was observed for U_{400}-As_{400} (Table 2), suggesting that the addition of As(V) inhibited the reduction of U(VI) to U(IV) by *M. circinelloides*. However, the amount of $UO_2HAsO_4 \cdot 4H_2O$ was increased with increasing As(V) dosage. For instance, 10.1 and 48.6% of $UO_2HAsO_4 \cdot 4H_2O$ were generated for U_{400}-As_{40} and U_{400}-As_{400}, respectively (Table 2).

Fig. 6b shows the U L_{III}-edge EXAFS data of U_{400}, U_{400}-As_{40}, U_{400}-As_{200} and U_{400}-As_{400}, and the fitted structural parameters (CN, R, and σ^2) were listed in Table 3. As shown in Fig. 6b, the different RSFs suggested the U in mycelia of *M. circinelloides* with different coordination structures. The first peak in the EXAFS spectra can be fitted by 2 axial oxygen atoms (U-O_{ax}) at an atomic distance of ~1.8 Å. Then, the second peak represented equatorial oxygen atoms (U-O_{eq}) at a distance of 2.32~2.36 Å. The different amount of O_{eq} (from 2 to 7) revealed the different interaction mechanism (Bernier-Latmani et al., 2010; Burns, 2005). For U_{400}, the third peaks can be fitted by U-C shell at ~2.88 Å, which indicated U(VI) was also coordinated to carbon-containing functional groups (Sun et al., 2016). The batch experiments showed that the concentration of organic acids produced by fungus was responsible for binding U(VI) and As(V). Lovley and Gorby (1992) demonstrated that a moderately acidophilic fungus (i.e., *Coniochaeta fodinicola*) effectively removed uranium from aqueous solution. For U_{400}-As_{400}, a strong peak can be fitted by U-As shell at ~3.68 Å, which was similar to the U-As shell of $UO_2HAsO_4 \cdot 4H_2O$ (Troyer et al., 2014a,b). Analogously, it was demonstrated that U(VI) and As(V) can generate U–As precipitates ($UO_2HAsO_4 \cdot 4H_2O$) on metal oxides (Tang et al., 2009; Troyer et al., 2014a,b). The four peak at ~3.94 Å can be fitted by U–U distance of $U^{(IV)}O_2(s)$, indicating that adsorbed U(VI) was partly reduced to U(IV) in higher U(VI) dosage (Bernier-Latmani et al.,

Table 2
Contents of various uranium species for U_{400}, U_{400}-As_{40}, U_{400}-As_{200} and U_{400}-As_{400} calculated from linear-combination fitting.

Samples	Nano-UO_2 (%)	Adsorbed U(VI) (%)	Trögerite (%)	R factor [a]
U_{400}	30.1	69.9	0	0.0012056
U_{400}-As_{40}	24.2	65.7	10.1	0.0003448
U_{400}-As_{200}	16	55.1	28.9	0.0001448
U_{400}-As_{400}	9.7	41.7	48.6	0.0005168

[a] The normalized sum of the difference between the model and the fit.

Table 3
Uranium L_{III}-edge EXAFS spectra for U(VI) accumulation by *M. circinelloides* at different As(V) conditions.

Samples	Shell	R(Å) [a]	CN [b]	σ^2 (Å^2) [c]
U_{400}	U–O_{ax}	1.88	2.04	0.025
	U–O_{eq}	2.32	7.05	0.009
	U-C	2.88	1.10	0.025
	U–U	3.94	9.67	0.009
U_{400}-As_{40}	U–O_{ax}	1.90	2.04	0.025
	U–O_{eq}	2.34	5.87	0.009
	U-As	3.68	1.90	0.008
	U–U	3.89	5.12	0.008
U_{400}-As_{200}	U–O_{ax}	1.82	2.02	0.006
	U–O_{eq}	2.35	5.10	0.007
	U-As	3.69	2.70	0.005
	U–U	3.92	4.70	0.006
U_{400}-As_{400}	U–O_{ax}	1.79	2.01	0.006
	U–O_{eq}	2.36	6.12	0.041
	U-As	3.68	3.60	0.005
	U–U	4.01	2.65	0.016

[a] R is the bond distance.
[b] CN is coordination numbers of neighbors.
[c] σ^2 is the Debye-Waller.

2010; Sun et al., 2016). The speciation of uranium in fungi mycelia by EXAFS analysis was consistent with XANES results. Bioreduction of U(VI) to U(IV) by microorganisms play a key role in controlling the immobilization and fate of U in surface sediments (Bernier-Latmani et al., 2010). Therefore, the biosynthesis of thiol compounds (NP-SH and PB-SH), the activation of antioxidant enzymes (SOD and CAT) and secretion of organic acids induced in *M. circinelloides* played a considerable role in responses to U(VI) and As(V) detoxification.

4. Conclusions

M. circinelloides isolated from radionuclides' contaminated soils displayed particular resistance to U(VI) and As(V) at low and middle-concentrations, moreover the enhanced immobilization of U(VI) on fungi mycelia was observed after addition of As(V). M. circinelloides dealing with U(VI) and As(V) stress was mainly attributed to the biosynthesis of thiol compounds (NP-SH and PB-SH), the activation of antioxidant enzymes (SOD and CAT), and secretion of organic acids (oxalic and citric acid). The results from XANES and EXAFS analysis indicated that U(VI) was mainly reduced to nano-uraninite (nano-UO_2), while As(V) hindered U(VI) reduction due to the formation of uranyl arsenate precipitate. These results are crucial for further understanding the transportation and fate of radionuclides and heavy metals on fungi in environmental cleanup.

Acknowledgments

This research was supported by National Natural Science Foundation of China (21607156, 21577093 and 91326202), China Postdoctoral Science Foundation funded project (2015M581047), the Fundamental Research Funds for the Central Universities (JB2015001), the Priority Academic Program Development of Jiangsu Higher Education Institutions, and the Collaborative Innovation Center of Radiation Medicine of Jiangsu Higher Education Institutions are acknowledged.

Appendix A. Supplementary data

Supplementary data related to this article can be found at https://doi.org/10.1016/j.envpol.2018.02.060.

References

Akhtar, K., Waheed Akhtar, M., Khalid, A.M., 2007. Removal and recovery of uranium from aqueous solutions by *Trichoderma harzianum*. Water Res. 41, 1366–1378.
Arwidsson, Z., Johansson, E., Kronhelm, T.V., Allard, B., Hees, P.V., 2010. Remediation of metal contaminated soil by organic metabolites from fungi i—production of organic acids. Water Air Soil Pollut. 205, 215–226.
Azevedo, M.M., Carvalho, A., Pascoal, C., Rodrigues, F., Cássio, F., 2007. Responses of antioxidant defenses to Cu and Zn stress in two aquatic fungi. Sci. Total Environ. 377, 233–243.
Baldrian, P., 2003. Interactions of heavy metals with white-rot fungi. Enzym. Microb. Technol. 32 (1), 78–91.
Bernier-Latmani, R., Veeramani, H., Vecchia, E.D., Junier, P., Lezama-Pacheco, J.S., Suvorova, E.I., Sharp, J.O., Wigginton, N.S., Bargar, J.R., 2010. Non-uraninite products of microbial U(VI) reduction. Environ. Sci. Technol. 44, 9456–9462.
Blake, J.M., Avasarala, S., Artyushkova, K., Ali, A.M.S., Brearley, A.J., Shuey, C., Hirani, C., 2015. Elevated Concentrations of U and Co-occurring metals in abandoned mine wastes in a Northeastern Arizona native American community. Environ. Sci. Technol. 49, 8506–8514.
Boriová, K., Urík, M., Bujdoš, M., Pifková, I., Matúš, P., 2016. Chemical mimicking of bio-assisted aluminium extraction by *Aspergillus niger's* exometabolites. Environ. Pollut. 218, 281–288.
Brooks, S.C., Fredrickson, J.K., Carroll, S.L., Kennedy, D.W., Zachara, J.M., Plymale, A.E., 2003. Inhibition of bacterial U(VI) reduction by calcium. Environ. Sci. Technol. 37, 1850–1858.
Burns, P.C., 2005. U^{6+} minerals and inorganic compounds: insight into an expanded structural hierarchy of crystal structures. Can. Mineral. 43, 1839–1894.
Chen, B.D., Zhu, Y.G., Smith, F.A., 2006. Effects of arbuscular mycorrhizal inoculation on uranium and arsenic accumulation by Chinese brake fern (*Pteris vittata L.*) from a uranium mining-impacted soil. Chemosphere 62, 1464–1473.
Das, N., 2012. Remediation of radionuclide pollutants through biosorption—an overview. CLEAN–Soil Air Water 40, 16–23.
Desouky, O.A., El-Mougith, A.A., Hassanien, W.A., Awadalla, G.S., Hussien, S.S., 2016. Extraction of some strategic elements from thorium–uranium concentrate using bioproducts of Aspergillus ficuum and Pseudomonas aeruginosa. ARAB J. Chem. 9, S795–S805.
Ding, C.C., Feng, S., Li, X., Liao, J., Yang, Y., An, Z., Wu, Q., Zhang, D., Yang, J., Tang, J., Zhang, J., Liu, N., 2014a. Mechanism of thorium biosorption by the cells of the soil fungal isolate *Geotrichum sp.* dwc-1. Radiochim. Acta 102, 175–184.
Ding, Y.Z., Song, Z.G., Feng, R.W., Guo, J.K., 2014b. Interaction of organic acids and pH on multi-heavy metal extraction from alkaline and acid mine soils. Int. J. Environ. Sci. Technol. 11, 33–42.
Ding, C.C., Cheng, W.C., Sun, Y.B., Wang, X.K., 2015. Effects of Bacillus subtilis on the reduction of U (VI) by nano-Fe^0. Geochem. Cosmochim. Acta 165, 86–107.
Dresel, P.E., Wellman, D.M., Cantrell, K.J., Truex, M.J., 2011. Review: technical and policy challenges in deep vadose zone remediation of metals and radionuclides. Environ. Sci. Technol. 45, 4207–4216.
El-Sayed, M.T., 2015. An investigation on tolerance and biosorption potential of *Aspergillus awamori* ZU JQ 965830.1 to Cd(II). Ann. Microbiol. 65, 69–83.
Gadd, G.M., 2010. Metals, minerals and microbes: geomicrobiology and bioremediation. Microbiology 156, 609–643.
Grąz, M., Jarosz-Wilkołazka, A., 2011. Oxalic acid, versatile peroxidase secretion and chelating ability of Bjerkandera fumosa in rich and limited culture conditions. World J. Microbiol. Biotechnol. 27, 1885–1891.
Grąz, M., Jarosz-Wilkołazka, A., Pawlikowska-Pawlęga, B., 2009. Abortiporus biennis tolerance to insoluble metal oxides: oxalate secretion, oxalate oxidase activity, and mycelial morphology. Biometals 22, 401–410.
Guimarães-Soares, L., Pascoal, C., Cássio, F., 2007. Effects of heavy metals on the production of thiol compounds by the aquatic fungi *Fontanospora fusiramosa* and *Flagellospora curta*. Ecotoxicol. Environ. Saf. 66, 36–43.
Gutiérrez, J.C., 2009. Heavy metals generate reactive oxygen species in terrestrial and aquatic ciliated protozoa. Comp. Biochem. Physiol. C Toxicol. Pharmacol. 149, 90–96.
Hansen, H.K., Ribeiro, A., Mateus, E., 2006. Biosorption of arsenic(V) with Lessonia nigrescens. Miner. Eng. 19, 486–490.
Harms, H., Schlosser, D., Wick, L.Y., 2011. Untapped potential: exploiting fungi in bioremediation of hazardous chemicals. Nat. Rev. Microbiol. 9, 177–192.
Li, N.J., Zeng, G.M., Huang, D.L., Hu, S., Feng, C.L., Zhao, M.H., Lai, C., Huang, C., Wei, Z., Xie, G.X., 2011. Oxalate production at different initial Pb^{2+} concentrations and the influence of oxalate during solid-state fermentation of straw with Phanerochaete chrysosporium. Bioresour. Technol. 102, 8137–8142.
Li, N., Zeng, G., Huang, D., Huang, C., Lai, C., Wei, Z., Xu, P., Zhang, C., Cheng, M., Yan, M., 2015. Response of extracellular carboxylic and thiol ligands (oxalate, thiol compounds) to Pb^{2+} stress in *Phanerochaete chrysosporium*. Environ. Sci. Pollut. Res. 22, 12655–12663.
Liber, K., Doig, L.E., White-Sobey, S.L., 2011. Toxicity of uranium, molybdenum, nickel, and arsenic to *Hyalella azteca* and *Chironomus dilutus* in water-only and spiked-sediment toxicity tests. Ecotoxicol. Environ. Saf. 74, 1171–1179.
Liu, D., Kottke, I., 2004. Subcellular localization of copper in the root cells of *Allium sativum* by electron energy loss spectroscopy (EELS). Bioresour. Technol. 94, 153–158.
Lovley, D.R., Gorby, Y.A., 1992. Enzymic uranium precipitation. Environ. Sci. Technol. 26, 205–207.
Mäkelä, M.R., Hildén, K., Lundell, T.K., 2010. Oxalate decarboxylase: biotechnological update and prevalence of the enzyme in filamentous fungi. Appl. Microbiol. Biotechnol. 87, 801–814.
Martin, G., Guggiari, M., Bravo, D., Zopfi, J., Cailleau, G., Aragno, M., Job, D., Verrecchia, E., Junier, P., 2012. Fungi, bacteria and soil pH: the oxalate–carbonate pathway as a model for metabolic interaction. Environ. Microbiol. 14, 2960–2970.
Montiel-Rozas, M.M., Madejón, E., Madejón, P., 2016. Effect of heavy metals and organic matter on root exudates (low molecular weight organic acids) of herbaceous species: an assessment in sand and soil conditions. Environ. Pollut. 216, 273–281.
O'Loughlin, E.J., Kelly, S.D., Kemner, K.M., 2010. XAFS investigation of the interactions of U(VI) with secondary mineralization products from the bioreduction of Fe(III) oxides. Environ. Sci. Technol. 44, 1656–1661.
Richard, A., Rozsypal, C., Mercadier, J., Banks, D.A., Cuney, M., Boiron, M.C., Cathelineau, M., 2012. Giant uranium deposits formed from exceptionally uranium-rich acidic brines. Nat. Geosci. 5, 142–146.
Rico, C.M., Morales, M.I., McCreary, R., Castillo-Michel, H., Barrios, A.C., Hong, J., Tafoy, A., Lee, W.Y., Varela-Ramirez, A., Peralta-Videa, J.R., Gardea-Torresdey, J.L., 2013. Cerium oxide nanoparticles modify the antioxidative stress enzyme activities and macromolecule composition in rice seedlings. Environ. Sci. Technol. 47, 14110–14118.
Rodríguez-Lado, L., Sun, G., Berg, M., Zhang, Q., Xue, H., Zheng, Q., Johnson, C.A., 2013. Groundwater arsenic contamination throughout China. Science 341, 866–868.
Schneider, J., Bundschuh, J., de Melo Rangel, W., Guilherme, L.R.G., 2017. Potential of different AM fungi (native from As-contaminated and uncontaminated soils) for supporting Leucaena leucocephala growth in As-contaminated soil. Environ. Pollut. 224, 125–135.
Schnug, E., Lottermoser, B.G., 2013. Fertilizer-derived uranium and its threat to

human health. Environ. Sci. Technol. 47, 2433–2434.
Sheng, G.D., Yang, P.J., Tang, Y.N., Hu, Q.Y., Li, H., Ren, X.M., Hu, B.W., Wang, X.K., Huang, Y.Y., 2016. New insights into the primary roles of diatomite in the enhanced sequestration of UO^{22+} by zerovalent iron nanoparticles: an advanced approach utilizing XPS and EXAFS. Appl. Catal. B Environ. 193, 189–197.
Sitte, J., Akob, D.M., Kaufmann, C., Finster, K., Banerjee, D., Burkhardt, E.M., Küsel, K., 2010. Microbial links between sulfate reduction and metal retention in uranium-and heavy metal-contaminated soil. Appl. Environ. Microbiol. 76, 3143–3152.
Song, W.C., Liang, J., Tao, W., Wang, X.X., Hu, J., Hayat, T., Wang, X.K., 2016a. Accumulation of Co(II) and Eu(III) by the mycelia of *Aspergillus niger* isolated from radionuclide-contaminated soils. Chem. Eng. J. 304, 186–193.
Song, W.C., Wang, X.X., Wen, T., Yu, S.J., Zou, Y.D., Sun, Y.B., Hayat, T., Wang, X.K., 2016b. Immobilization of As(V) in *Rhizopus oryzae* investigated by batch and XAFS techniques. ACS Omega 1, 899–906.
Srivastava, S., Thakur, I.S., 2006. Biosorption potency of *Aspergillus niger* for removal of chromium (VI). Curr. Microbial 53, 232–137.
Stylo, M., Alessi, D.S., Shao, P.P., Lezama-Pacheco, J.S., Bargar, J.R., Bernier-Latmani, R., 2013. Biogeochemical controls on the product of microbial U (VI) reduction. Environ. Sci. Technol. 47, 12351–12358.
Sun, Y.B., Li, J.X., Wang, X.K., 2014. The retention of uranium and europium onto sepiolite investigated by macroscopic, spectroscopic and modeling techniques. Geochem. Cosmochim. Acta 140, 621–643.
Sun, Y.B., Wu, Z.Y., Wang, X.X., Ding, C.C., Cheng, W.C., Yu, S.H., Wang, X.K., 2016. Macroscopic and microscopic investigation of U(VI) and Eu(III) adsorption on carbonaceous nanofibers. Environ. Sci. Technol. 50, 4459–4467.
Tang, Y., McDonald, J., Reeder, R.J., 2009. Enhanced uranium sorption on aluminum oxide pretreated with arsenate. Part II: spectroscopic studies. Environ. Sci. Technol. 43, 4452–4458.
Troyer, L.D., Tang, Y., Borch, T., 2014a. Simultaneous reduction of arsenic(V) and uranium(VI) by mackinawite: role of uranyl arsenate precipitate formation. Environ. Sci. Technol. 48, 14326–14334.
Troyer, L.D., Stone, J.J., Borch, T., 2014b. Effect of biogeochemical redox processes on the fate and transport of as and u at an abandoned uranium mine site: an x-ray absorption spectroscopy study. Environ. Chem. 11, 18–27.
Ulrich, K.U., Singh, A., Schofield, E.J., Bargar, J.R., Veeramani, H., Sharp, J.O., Bernier-Latmani, R., Giammar, D.E., 2008. Dissolution of biogenic and synthetic UO_2 under varied reducing conditions. Environ. Sci. Technol. 42, 5600–5606.
Vázquez-Campos, X., Kinsela, A.S., Collins, R.N., Neilan, B.A., Aoyagi, N., Waite, T.D., 2015. Uranium binding mechanisms of the acid-tolerant fungus *Coniochaeta fodinicola*. Environ. Sci. Technol. 49, 8487–8496.
Wall, J.D., Krumholz, L.R., 2006. Uranium reduction. Annu. Rev. Microbiol. 60, 149–166.
Wang, Y.D., Li, G.Y., Ding, D.X., Zhou, Z.X., Deng, Q.W., Hu, N., Tan, Y., 2013. Uranium leaching using mixed organic acids produced by *aspergillus niger*. J. Radioanal. Nucl. Chem. 298, 769–773.
Wei, Z., Hillier, S., Gadd, G.M., 2012. Biotransformation of manganese oxides by fungi: solubilization and production of manganese oxalate biominerals. Environ. Microbiol. 14, 1744–1753.
Wu, W.M., Carley, J., Gentry, T., Ginder-Vogel, M., Fienen, M., Mehlhorn, T., 2006. Pilot-scale in situ bioremedation of uranium in a highly contaminated aquifer. 2. Reduction of U(VI) and geochemical control of U(VI) bioavailability. Environ. Sci. Technol. 40, 3986–3995.
Wu, W.M., Carley, J., Luo, J., Ginder-Vogel, M., Cardenas, E., Leigh, M., Hwang, C., Kelly, S., Ruan, C., Wu, L., 2007. In situ bioreduction of uranium(VI) to submicromolar levels and reoxidation by dissolved oxygen. Environ. Sci. Technol. 41, 5716–5723.
Xu, H., Song, P., Gu, W., Yang, Z., 2011. Effects of heavy metals on production of thiol compounds and antioxidant enzymes in *Agaricus bisporus*. Ecotoxicol. Environ. Saf. 74, 1685–1692.
Xu, P., Liu, L., Zeng, G., Huang, D., Lai, C., Zhao, M., Zhang, C., 2014. Heavy metal-induced glutathione accumulation and its role in heavy metal detoxification in *Phanerochaete chrysosporium*. Appl. Microbiol. Biotechnol. 98, 6409–6418.
Xu, P., Leng, Y., Zeng, G., Huang, D., Lai, C., Zhao, M., Wen, Z., Li, N., Huang, C., Zhang, C., Li, F., Cheng, M., 2015. Cadmium induced oxalic acid secretion and its role in metal uptake and detoxification mechanisms in *Phanerochaete chrysosporium*. Appl. Microbiol. Biotechnol. 99, 435–443.
Xu, X., Xia, L., Chen, W., Huang, Q., 2017. Detoxification of hexavalent chromate by growing *Paecilomyces lilacinus* XLA. Environ. Pollut. 225, 47–54.
Yin, Y., Yang, X., Hu, L., Tan, Z., Zhao, L., Zhang, Z., Liu, J., Jiang, G., 2016. Superoxide-mediated extracellular biosynthesis of silver nanoparticles by the fungus Fusarium oxysporum. Environ. Sci. Technol. Lett. 3, 160–165.
Zhan, F., He, Y., Li, Y., Li, T., Yang, Y.Y., Toor, G.S., Zhao, Z., 2015. Subcellular distribution and chemical forms of cadmium in a dark septate endophyte (DSE), Exophiala pisciphila. Environ. Sci. Pollut. Res. 22, 17897–17905.
Zhang, X.H., Zhu, Y.G., Chen, B.D., Lin, A.J., Smith, S.E., Smith, F.A., 2005. Arbuscular mycorrhizal fungi contribute to resistance of upland rice to combined metal contamination of soil. J. Plant Nutr. 28, 2065–2077.
Zhang, S., Zhang, X., Chang, C., Yuan, Z., Wang, T., Zhao, Y., Zhang, Z., 2016. Improvement of tolerance to lead by filamentous fungus *Pleurotus ostreatus* HAU-2 and its oxidative responses. Chemosphere 150, 33–39.
Zhu, Y., Zhuang, L., Goodell, B., Cao, J., Mahaney, J., 2016. Iron sequestration in brown-rot fungi by oxalate and the production of reactive oxygen species (ros). Int. Biodeterior. Biodegrad. 109, 185–190.